analytical chemistry

pubs.acs.org/ac Article

Anti-Fouling Magnetic Beads Combined with Signal Amplification Strategies for Ultra-Sensitive and Selective Electrochemiluminescence Detection of MicroRNAs in Complex Biological Media

Qiuxia Hao, Qingzhang Xu, Shuyan Niu, Caifeng Ding,* and Xiliang Luo*

Cite This: *Anal. Chem.* 2021, 93, 10679−10687 Read Online

ACCESS | Metrics & More | Article Recommendations | Supporting Information

ABSTRACT: Herein, an electrochemiluminescence (ECL) microRNA biosensor based on anti-fouling magnetic beads (MBs) and two signal amplification strategies was developed. The newly designed anti-fouling dendritic peptide was wrapped on the surfaces of MBs to make them resistant to nonspecific adsorption of biomolecules in complex biological samples so as to realize accurate and selective target recognition. One of the amplification strategies was achieved through nucleic acid cycle amplification based on the DNAzyme on the surfaces of MBs. Then, the output DNA generated by the nucleic acid cycle amplification program stimulated the hybrid chain reaction (HCR) process on the modified electrode surface to generate the other amplification of the ECL response. Titanium dioxide nanoneedles (TiO_2 NNs), as a co-reaction accelerator of the $Ru(bpy)_2(cpaphen)^{2+}$ and tripropylamine (TPrA) system, were wrapped with the electrodeposited polyaniline (PANI) on the electrode surface to enhance the ECL intensity of $Ru(bpy)_2(cpaphen)^{2+}$. The conducting polymer PANI can not only immobilize the TiO_2 NNs but also improve the conductivity of the modified electrodes. The biosensor exhibited ultra-high sensitivity and excellent selectivity toward the detection of miRNA 21, with a detection limit of 0.13 fM. More importantly, with the anti-fouling MBs as a unique separation tool, this ECL biosensor was capable of assaying targets in complex biological media such as serum and cell lysate.

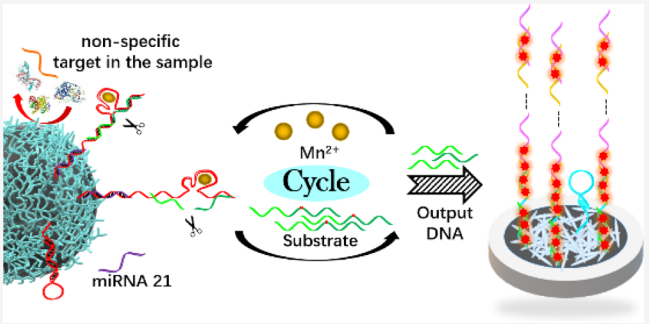

INTRODUCTION

As a short single-stranded endogenous RNA, the microRNA (miRNA) plays an indispensable regulatory role in many life processes. It regulates various life processes, for instance, tissue differentiation, stem cell self-renewal, and cell growth. The need for extensive research in various physiological or pathological processes is very urgent due to its involvement in the occurrence and metastasis of cancer.[1−3] Many reported studies have shown that it can serve as a tool for disease diagnosis or patient prognosis as well as a biomarker or treatment tool in the clinic.[4,5] However, due to its high sequence similarity, small size, and low abundance, the development of simple and efficient analysis strategies still faces huge challenges.

Classical PCR amplification and microarrays are traditional miRNA analysis strategies.[6−10] In recent years, analysis strategies for miRNA research such as surface-enhanced Raman, miRNA imaging, electrochemiluminescence (ECL) sensors, and electrochemical sensors have also been reported.[11−17] However, due to the similarity of homologous miRNAs and the problems of trace amounts in biological samples, these methods inevitably suffer from miRNA detection errors, low sensitivity, or complicated operations. Therefore, the introduction of signal amplification design in the detection system has become a crucial step. So far, most signal amplification strategies are based on target conversion, such as nuclease-assisted nucleic acid cycle amplification and hybrid chain reaction (HCR) without enzyme participation.[18−21] Since the suitable reaction conditions for enzymes are usually very strict, target signal amplification without enzyme participation has attracted more and more attention from scientists. As expected, a DNAzyme, as a nucleic acid cut by metal ions, becomes a perfect choice to replace nucleases.[22−25]

As an analysis strategy with simple operation, high sensitivity, and strong response controllability, ECL has been extensively used in clinical analysis and research.[26,27] In order

Received: May 25, 2021
Accepted: July 9, 2021
Published: July 21, 2021

https://doi.org/10.1021/acs.analchem.1c02186
Anal. Chem. 2021, 93, 10679−10687

Scheme 1. Modification Process of Anti-Fouling MBs and Nucleic Acid Cycle Amplification Program (A); the Electronic Sensing Process (B) of the Designed ECL Biosensor

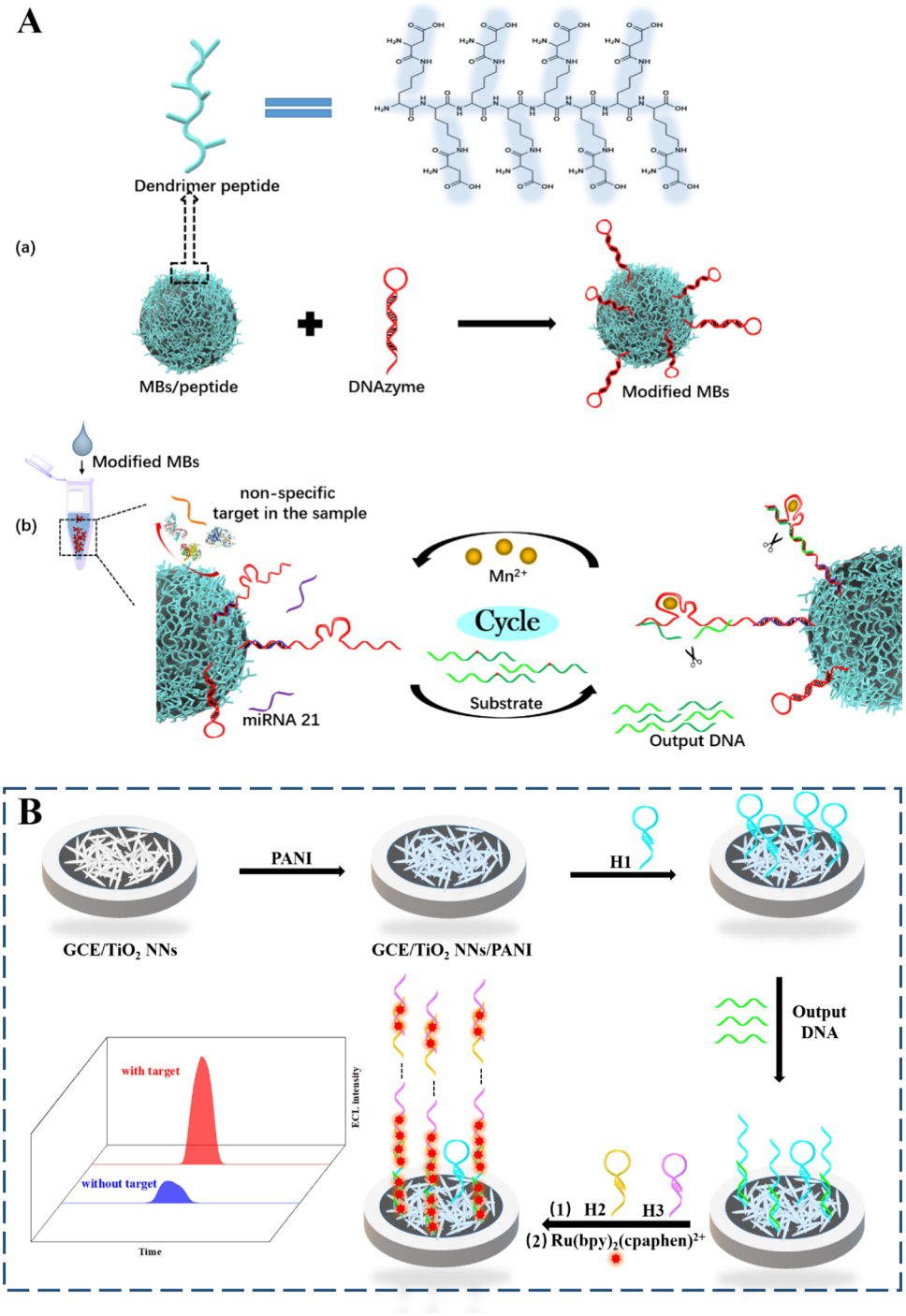

to further improve the response efficiency of the target, Yuan's group prepared many materials to enhance the ECL intensity.[28−32] In 2019, they reported that TiO_2 NNs, as a co-reaction promoter of the classic combination of Ru-$(bpy)_2(cpaphen)^{2+}$ and TprA, can enhance the ECL intensity greatly. However, the poor electrical conductivity of the TiO_2 NNs and the lack of modified groups on the surface limit its application in ECL sensors.

In biological real samples, false positives or false negatives caused by nonspecific adsorption of impurities such as proteins are also an important problem in many sensor analysis systems. Therefore, the concept of anti-fouling has become an important part of the sensor analysis strategy. So far, there have been many reports on materials with anti-fouling properties such as betaine polymers, peptides, and BSA composite anti-fouling layers.[33−38] Among them, peptides as natural amphiphiles with excellent biocompatibility have become a research hotspot. Due to the strong hydration capacity of the peptide, it can resist nonspecific adsorption in complex biological environments. By adjusting the type and quantity of amino acids to make the peptide neutral, the nonspecific adsorption of proteins due to electrostatic

https://doi.org/10.1021/acs.analchem.1c02186
Anal. Chem. 2021, 93, 10679−10687

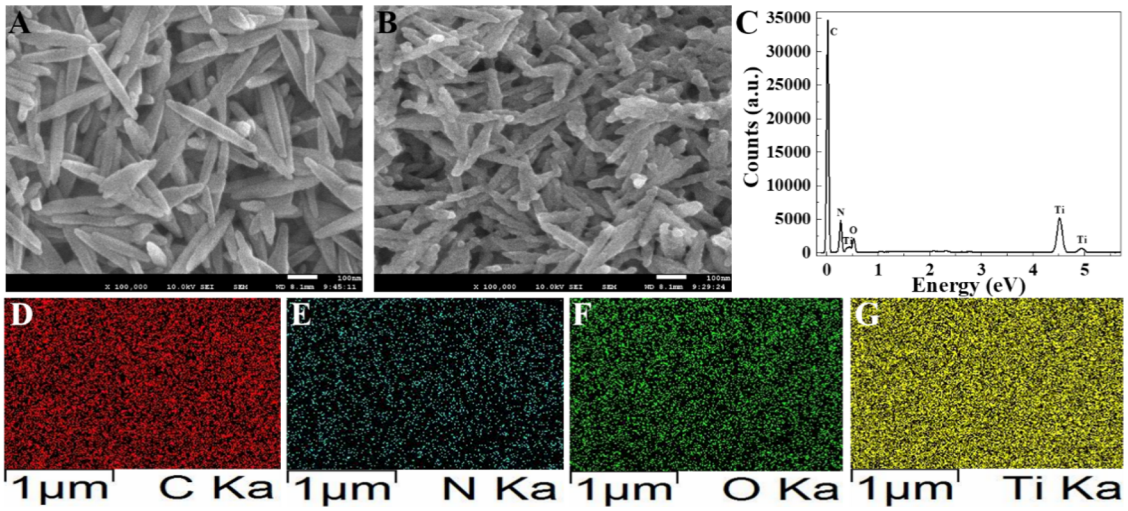

Figure 1. SEM image of TiO_2 NNs/GCE (A) and TiO_2 NNs/PANI/GCE (B). The EDX element analysis (C). SEM−EDX element mapping (D−G) of TiO_2 NNs/PANI/GCE.

attraction can be avoided.[39,40] In recent years, our group has developed a series of quantitative biosensors with anti-fouling properties based on peptides for detecting biomolecules in real samples.[41−47]

Herein, we proposed an ECL biosensor based on a newly designed sequence of dendrimer peptide and dual signal amplification mechanism for analysis of miRNA 21, as depicted in Scheme 1. Magnetic beads (MBs) were modified with the hairpin structure DNAzyme and dendritic peptides. In the presence of miRNA 21, the hairpin structure of the DNAzyme is opened through the hybridization between miRNA and its complementary part of the DNAzyme modified on the surface of the anti-fouling MBs. Then another part of the single-stranded region of the opened DNAzyme chain hybridizes with the substrate to become a three-chain structure, including a folding recognition sequence and a cleavage site related to Mn^{2+}. In the presence of Mn^{2+}, the substrate strands were cleaved and dissociated from the three-chain structure to produce a short single strand as output DNA. Then, another substrate chain could hybridize with the single-stranded region dissociated from the old substrate to form a new three-chain structure and so on. Due to the first amplification of the DNAzyme-based nucleic acid cycle amplification program, a lot of output DNA was obtained to open H1 on the sensing interface of the modified electrode, and subsequently, the HCR process occurred with the participation of the H2 and H3 to form a long double-stranded DNA. Next, the positively charged $Ru(bpy)_2(cpaphen)^{2+}$ was inserted into double-stranded DNA with a large amount of negative charge by electrostatic adsorption to generate the ECL signal to realize the second signal amplification. In addition, the electrode surface was modified with TiO_2 NNs/PANI to enhance the ECL signal and improve the conductivity of the modified electrode. Due to the double amplification of the strategy, the biosensor realized high-sensitivity analysis of miRNA 21 and also showed a satisfactorily high anti-fouling analysis performance in the actual sample analysis.

EXPERIMENTAL SECTION

Modification of Anti-Fouling MBs. 20 μL of MBs modified with the carboxyl group was washed three times, and then 40 μL of imidazole hydrochloric acid buffer containing 0.8 M EDC and 0.2 M NHS was added to activate the carboxyl groups for 1 h. After magnetic separation, 20 μL of dendritic peptide (0.2 g/mL) was added and incubated overnight. The dendritic peptide-modified MBs were dispersed in 40 μL of PBS including EDC (1 mg/mL) and NHS (1 mg/mL) for 1 h to activate the carboxyl group of the dendritic peptide. At last, 20 μL of DNAzyme was added and reacted overnight to connect it to the peptide by amide bonds.

Cycle Amplification Reaction Based on the DNAzyme. After cleaning the modified MBs three times, 20 μL of different concentrations of target was added and incubated for 2 h. After magnetic separation and washing three times, 20 μL of substrate (10^{-6} M) was added for cyclic hybridization reaction for 5 h. The DNA buffer for this process contained 5 mM Mn^{2+}. Then the MBs were discarded through magnetic separation to obtain a solution containing the output DNA.

Step-by-Step Assembly of the Biosensor. All GCEs were polished with alumina before use according to reported studies. First, 5 μL of TiO_2 NNs (the synthesis steps were provided in the Supporting Information) was applied to the GCE and dried naturally. Next, the PANI film was coated on the TiO_2 NN surface by galvanostatic electrodeposition technology at a constant current density of 0.01 mA/cm^2 for 10 min in 5 mL of an aqueous solution containing 406 μL of $HClO_4$, 45.6 μL of aniline, and 0.05 g of PSS as the stabilizer. Next, the carboxyl groups of H1 (10^{-6} M) were activated with EDC and NHS for 1 h. Finally, it was dropped onto the modified GCE surface and incubated overnight to connect to PANI by amide bonds.

ECL Analysis Procedures of miRNA 21. The output DNA produced by the above cyclic amplification process was added to the formed GCE surface for 2 h for hybridization reaction. After rinsing the electrode, the mixed solution containing H2 and H3 (10^{-6} M) was dripped onto the modified GCE for 2 h for HCR reaction. Then 1 μM $Ru(bpy)_2(cpaphen)^{2+}$ was dripped onto the sensing interface and incubated for 4 h, and the electrode was washed with PBS. The voltage range of ECL detection was 0 to 1.25 V, and the photomultiplier tube voltage was 800 V.

Polyacrylamide Gel Electrophoresis (PAGE) Analysis. All DNA (10^{-5} M) were heated to 95 °C, maintained for 5 min, and then slowly cooled to room temperature before use.

https://doi.org/10.1021/acs.analchem.1c02186
Anal. Chem. 2021, 93, 10679−10687

PAGE experiments were performed with 17.5% PAGE (4.256 mL H_2O, 3.5 mL 40% Acry/Bis, 160 μL 50 × TAE, 80 μL Aps (10%), 4 μL TEMED). In 1 × TAE solution, the voltage was maintained at 170 V for 5 min and then at 110 V for 90 min. Next, the gel was stained with EB solution (0.585 g NaCl, 100 mL H_2O, 30 μL EB) for 40 min, and then photographs were taken under an electrophoresis apparatus.

RESULTS AND DISCUSSION

Morphology Characterization and Optimization of New Composite TiO_2 NNs. The acicular nanomaterial was characterized by TEM and SEM. As shown in Figure S1, TiO_2 NNs had a standard needle-like structure and a uniform length of about 400 nm, which was consistent with the reported research. This indicated the successful synthesis of TiO_2 NNs. Irregular protrusions appeared on the surface of TiO_2 NNs coated with PANI (Figure 1A,B). The appearance of C and N elements in Figure 1C proved the formation of PANI on the surface of TiO_2 NNs. Meanwhile, the visual distribution of C, N, O, and Ti elements shown in Figure 1D−G also illustrates the successful uniform packing of PANI. Therefore, the new composite nanomaterials had been successfully prepared and the composite materials still maintained the standard needle-like structure.

Characterization of the MB Modification Process and Nucleic Acid Cycle Program. The modified MBs were characterized by TEM and zeta potential. A layer of obvious adhesion was observed on the surface of the MBs modified with dendritic peptide (Figure S2B) and the further modification of DNA (Figure S2C) compared with bare MBs (Figure S2A). At the same time, the successive appearance of N and P elements in the corresponding EDX element analysis spectrum also proved the successful modification of dendritic peptide and DNA on MBs (D, E). As displayed in Figure S3, the bare MBs were electronegative due to the carboxyl groups on the surface. Then they became electrically neutral when the dendritic peptide was modified. With the further modification of DNA, the modified MBs were in an electronegative state due to the negative charge of DNA. These results further proved the successful modification of dendritic peptide and DNA on MBs.

The nucleic acid cycle hybridization process was verified by PAGE. Considering the poor stability of RNA in vitro, a synthetic DNA target was used instead of miRNA 21 for PAGE experiments. As shown in Figure 2A, the DNAzyme, target DNA, and substrate strand correspond to lane 1 to lane 3, respectively. A significantly higher band representing the hybridization of the DNAzyme and target DNA was observed in lane 4. Two obvious bands were observed in the mixture of the DNAzyme and substrate (lane 5) and the mixture of the substrate and target DNA (lane 6), proving that no hybridization reaction occurred. This proved that the calculation cycle cannot be performed without target DNA. When the three strands were mixed, a higher band representing the hybridization of the three strands was observed, and the other band was the redundant DNAzyme (lane 7). Compared with lane 7 without Mn^{2+}, the highest band of triple-strand hybridization in lane 8 with Mn^{2+} disappeared and a band with the same height as lane 4 appeared. More importantly, a band representing the output DNA generated by the cutting of the substrate strand appeared in the lowest position. This proved the success of the nucleic acid cycle amplification program based on the DNAzyme. Next, the HCR process was verified by the PAGE experiment. As depicted in Figure 2B, H1, H2, and H3 correspond to lanes 1 to 3, respectively. No new bands were observed for the mixture of three hairpin DNAs, indicating that the HCR process cannot occur without the target DNA (lane 4). When the output DNA generated by the nucleic acid cycle amplification process was added, a large ladder-like band appeared in lane 5, which proved the success of the HCR process. Therefore, the results of PAGE experiments proved the perfect feasibility of the designed nucleic acid cycle amplification program and HCR process. This allowed our strategy to have lower background and detection limits.

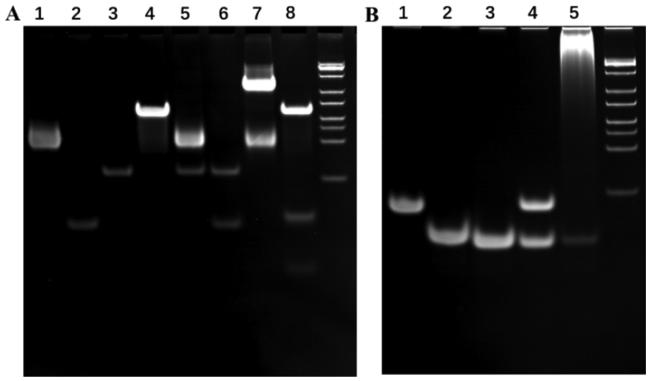

Figure 2. Gel electrophoresis image of the nucleic acid cycle process (A): lane 1, DNAzyme; lane 2, target DNA; lane 3, substrate; lane 4, DNAzyme + target DNA; lane 5, DNAzyme + substrate; lane 6, substrate + target DNA; lane 7, DNAzyme + target DNA + substrate; lane 8, DNAzyme + target DNA + substrate + Mn^{2+}; and the HCR process (B): lane 1, H1; lane 2, H2; lane 3, H3; lane 4, H1 + H2 + H3; lane 5, H1 + H2 + H3 + output DNA.

Anti-Fouling Performance of Dendritic Peptide-Encapsulated MBs. The most basic requirements for a peptide to have anti-fouling properties are to be electrically neutral and have good hydrophilicity. The hydrophilic property of the dendritic peptide was explored through static water contact angle experiments (Figure 3A,B and Table 1). Since the MBs are modified with carboxyl groups, a lower water contact angle appeared. The water contact angle value was still small after the peptide was wrapped, which proved that the dendritic peptide can form a surface with electrical neutralization and good hydrophilicity. To evaluate the anti-fouling property of the sensing strategy, protein attachment to the dendritic peptide modified MBs was carried out by using FITC-fluorescein-modified BSA (BSA-FITC) as an attachment model. The fluorescence intensities of the BSA-FITC solution before and after the incubation with the dendritic peptide modified MBs and naked MBs were measured. As depicted in Figure 3A, the fluorescence signal intensity of the MBs/peptide supernatant (curve b) decreases by only 5.5%, which was very similar to the fluorescence signal intensity of the BSA-FITC stock solution (curve a). However, the fluorescence signal of the supernatant of the bare MBs decreases by nearly 41.8% compared with the original solution. These results show that after the MBs were modified with dendritic peptide, the ability to prevent nonspecific adsorption of impurities was significantly enhanced.

To verify the anti-fouling ability of the MBs/peptide in real complex samples, the recovery rates of standard addition in three different complex environments of FBS, human serum, and HeLa cell lysate were also researched. As depicted in Table

https://doi.org/10.1021/acs.analchem.1c02186
Anal. Chem. 2021, 93, 10679−10687

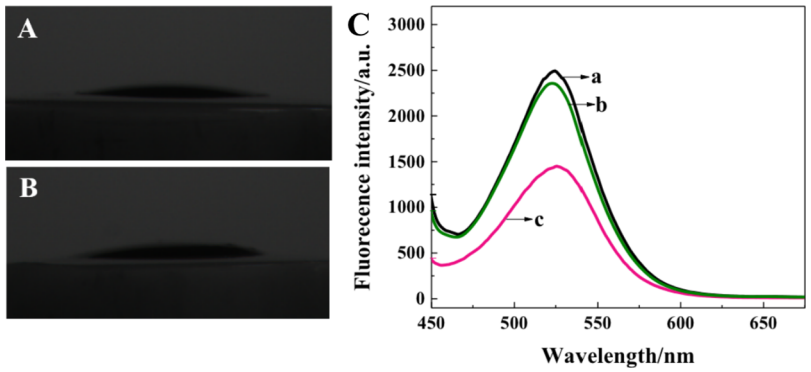

Figure 3. Water contact angle diagrams of MBs (A) and MBs/peptide (B); characterization of the anti-fouling performance of dendritic peptide-coated MBs by using BSA-FITC as an attachment model (C), the fluorescence intensities of the BSA-FITC solution before (a) and after incubation with the modified MBs (b) and naked MBs (c).

Table 1. Static Water Contact Angles of Different Surfaces

	surface contact angle (°)	
point	MBs	MBs/peptide
1	15.96	15.70
2	15.15	16.02
3	16.43	15.11
average	15.85	15.61

2, the MBs/peptide experimental group obtained very ideal recovery rates in FBS and human serum samples in contrast

Table 2. Comparison of the MBs Modified with or without Peptide in Complex Matrices

	MBs			MBs/peptide		
	added (pM)	found (pM)	recovery (%)	added (pM)	found (pM)	recovery (%)
FBS (40%)	0.1	0.08	80.0	0.1	0.09	90.0
	1.0	0.81	81.0	1.0	0.93	93.0
	10.0	7.63	76.3	10.0	91.5	91.5
human serum (40%)	0.1	0.07	70.0	0.1	0.09	90.0
	1.0	0.76	76.0	1.0	0.92	92.0
	10.0	8.21	82.1	10.0	9.28	92.8
cell lysate	0.1	0.09	90.0	0.1	0.11	110.0
	1.0	0.92	92.0	1.0	1.12	112.0
	10.0	9.36	93.6	10.0	10.81	108.1

with the bare MBs. This difference may be ascribed to the adhesion of impurities on the bare MBs, which increased steric hindrance and hindered the nucleic acid recognition process on the surface. Because there is a few amount of miRNA 21 existing in HeLa cells, the recovery rates of the two sets of experiments conducted in the HeLa cell lysate are both higher, especially the recovery rate of the anti-fouling MB group, exceeding 100%. In summary, these results indicated that the MBs/peptide had good anti-fouling performance due to the presence of the dendritic peptide layer.

Characterization of Electrode Construction and ECL Enhancement of TiO_2 NNs. The step-by-step construction of the biosensor was verified by cyclic voltammetry (CV) as exhibited in Figure 4A. Due to the poor conductivity of TiO_2 NNs, the redox peak current signal of the TiO_2 NNs/GCE (curve b) is lower than that of the bare GCE (curve a). After the formation of the PANI film on the surface of TiO_2 NNs/GCE, the current signal enhanced significantly (curve c) because of the excellent conductivity of PANI. With the further modification of negatively charged DNA, the current signal has a further decrease (curve d). This is due to the mutual repulsion of the same charges, which prevents the electron transition between $[Fe(CN)_6]^{3-/4-}$ and sensing surface.

The stepwise construction of the biosensor was also verified through electrochemical impedance spectra (EIS). As displayed in Figure 4B, the electrode modified with TiO_2 NNs (curve b) showed a larger semicircle in the EIS spectrum in contrast with the bare GCE (curve a). After the electrodeposition of the PANI film, the diameter of the semicircle in the spectrum decreased significantly (curve c). When the DNA strand was assembled on the electrode, the diameter of the semicircle increased (curve d). This result completely matches with the result of CV and further proves the successful construction of the designed ECL sensor.

Figure 4C shows that the current signal of the 50th circle decreased by only 9.1% compared with the first circle after 50 consecutive CV scans of the assembled sensor, which proves the high stability of the designed biosensor.

In order to verify the performance of the synthesized TiO_2 NNs for ECL signal enhancement, we compared the responses of sensors with (curve b) and without (curve a) TiO_2 NNs in the same concentration target. As displayed in Figure 4D, the ECL strength of curve b is almost twice as strong as that of curve a, showing great enhancement of TiO_2 NNs.

Optimization of the Experimental Conditions. The polymerization time of PANI was optimized as shown in Figure 3F. The ECL signal of the modified electrode increased at the first 10 min and then decreased slightly to an equilibration step. The significant signal increase describes the excellent conductivity of PANI. Nevertheless, with the continuous increase of the thickness of the PANI film, the ECL enhancement of TiO_2 NNs is hindered and the ECL signal decreases. Therefore, 10 min is chosen as the best electropolymerization time for PANI.

The concentration of capture DNA is crucial for detection, so the concentrations of DNAzyme modified on the surface of MBs and H1 modified on the surface of the electrode were optimized. With the increase of DNA concentration, the ECL signals gradually increased at first and then decreased a little and got a flat eventually as shown in Figure S5A,B. The optimal concentrations of DNAzyme and H1 were 20 and 1 μM, respectively. Considering that the density of DNA connected to the electrode surface will affect the recognition process and thus the response of the sensor, the density of

https://doi.org/10.1021/acs.analchem.1c02186
Anal. Chem. 2021, 93, 10679−10687

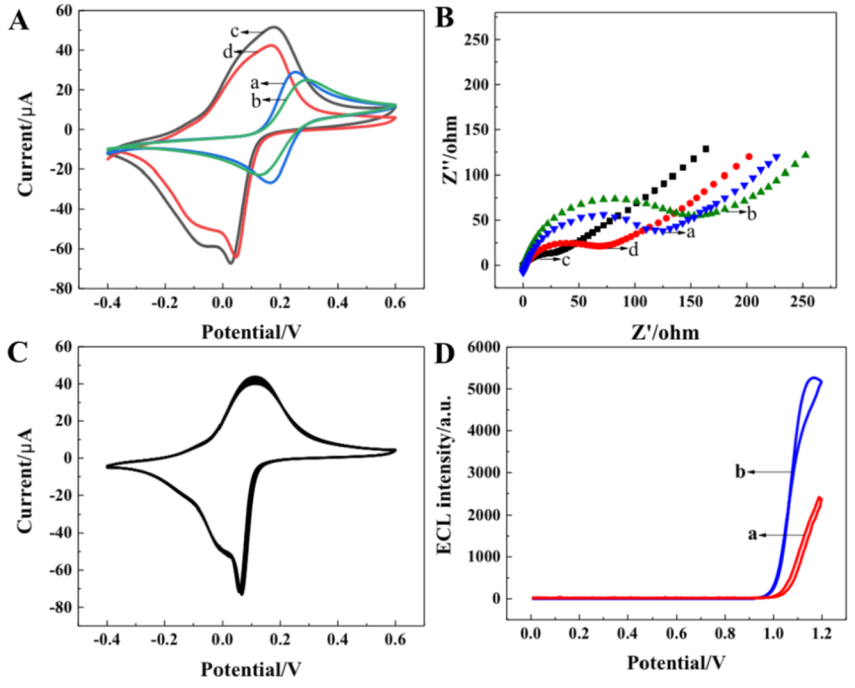

Figure 4. CV (A) and EIS (B) responses of the stepwise assembly procedure of the constructed sensor: (a) bare GCE, (b) GCE/TiO_2 NNs, (c) GCE/TiO_2 NNs/PANI, (d) GCE/TiO_2 NNs/PANI/DNA; the stability of the constructed electrode in 0.1 M PBS containing 5.0 mM $[Fe(CN)_6]^{3-/4-}$ (C); ECL signal response of $Ru(bpy)_2(cpaphen)^{2+}$ with and without TiO_2 NN modification in PBS (0.1 M, pH = 7.4) containing 10 mM TPrA (D).

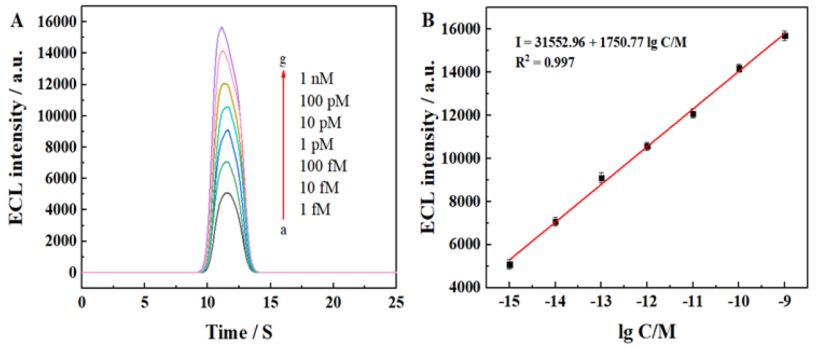

Figure 5. ECL response to different concentrations: 1 fM, 10 fM, 100 fM, 1 pM, 10 pM, 100 pM, and 1 nM targets in 0.1 M PBS containing 10 mM TPrA (A) and calibration plot of the ECL signal strength and the logarithmic value of $C_{miRNA\ 21}$ (B).

DNA connected to the electrode surface and its influence were further explored. To calculate the density of DNA probes on the capture DNA modified electrode surface, H1* (H1 tagged with the FAM fluorophore) was employed to replace H1 and the density of the H1* immobilized onto the GCE/TiO_2 NNs/PANI was calculated to be about 2.30×10^{14} strands/cm^2 (Supporting Information, Part 9). Obviously, the density of the DNA probes on the capture DNA modified electrode surface was consistent with the concentration of the H1 used to immobilization on the electrode. As shown in Figure S5 in the Supporting Information, the ECL intensity increased upon increasing the concentration from 1.0×10^{-8} to1.0×10^{-6} M, and then it started to decline. The density at the optimal concentration is about 10^{-6} M. The possible reason is that increasing the density of the capture probe could capture more output DNA to open H1 on the sensing interface and subsequently obtain more long double-stranded DNA through the HCR process with the participation of the H2 and H3. The ECL intensity increased consequently. However, too much H1 will hinder the recognition and binding processes on the electrode surface due to the steric hindrance, which will reduce the ECL signal obtained by the high concentration (density) of H1.

Analytical Performance of the Highly Sensitive Biosensor. Figure 5A shows the ECL intensities of different concentrations of miRNA 21 from 1 fM to 1 nM. We can see that the ECL response strength increases significantly with the increase of the amount of target. The ECL signal intensity had a satisfactory linear correlation with the logarithm of $C_{miRNA\ 21}$ (Figure 5B). The linear equation was $I = 31552.96 + 1750.77$ lg C with a detection limit (LOD) of 0.13 fM based on $3.3\sigma/k$. Compared with the reported works on miRNA 21 analysis as exhibited in Table 3, the designed analysis strategy has a wider response range and lower detection limit.

In order to highlight the superiority of the dual signal amplification strategy, we evaluated the biosensor response performance of the single signal amplification strategy. Because the ECL signal source $Ru(bpy)_2(cpaphen)^{2+}$ generates signals

https://doi.org/10.1021/acs.analchem.1c02186
Anal. Chem. 2021, 93, 10679−10687

Table 3. Comparison of This Analysis Strategy with Reported Works for miRNA 21 Detection

detection method	linear range	LOD	ref
electrochemical	0.10 nM to 10.0 nM	5 pM	48
fluorescence	20 pM to 10 nM	8 pM	49
ECL	2 fM to 100 pM	0.4 fM	50
photoluminescence	10 fM to 500 fM	3.0 fM	51
ECL	1 fM to 1 nM	0.13 fM	this work

by intercalating into the dsDNA, if there is no HCR process, too short dsDNA cannot load enough $Ru(bpy)_2(cpaphen)^{2+}$, which makes the sensor unable to respond effectively. Therefore, although the HCR reaction is also a kind of amplification process, the control experiment with and without the HCR process was not carried out in the comparative experiment. In the experimental group with only TiO_2 NNs and no DNAzyme cycle amplification, we designed a cycle-free nucleic acid hybridization sequence (Scheme S1). First, the DNA hybridization reaction of the process was verified by gel electrophoresis experiments. As shown in Figure S8, the H1' can be opened only when the target exists and the HCR process was initiated, which proved the feasibility of the designed DNA hybridization process. The two single amplification mode sensors with only DNAzyme cyclic and only TiO_2 NN enhanced amplification had linear responses in ranges of 40 fM to 25 pM and 50 fM to 13 pM, respectively (Figures S9A and Figures S10A). The linear equations were $I = 22979.6 + 1579.4 \lg(c/M)$ and $I = 25573.1 + 1640.92 \lg(c/M)$, with LODs of 4.2 and 5.6 fM (S/N = 3), respectively (Figures S9B and Figures S10B). Compared with the single signal amplification strategy, the biosensor of the dual signal amplification strategy can respond in a wider linear range and obtain a lower detection limit. This enables the constructed biosensor to realize more sensitive analysis and detection of miRNA 21 and is expected to realize early diagnosis of diseases.

Stability and Selectivity of the Biosensor. For the purpose of evaluating the stability of the ECL signal response, the signal strength was first evaluated by continuous ECL measurement in 0.1 M PBS containing 10 mM TPrA. As shown in Figure 6A, the ECL signal remained nearly unchanged after 25 cycles and the relative standard deviation (RSD) was 2.4%. In addition, the biosensor remained >90% of its original ECL response after being stored at 4 °C in PBS for 20 days and the RSD was 3.1% (Figure 6B). The above results proved that the assembled sensor had very high stability in both signal response and long-term storage. To investigate the selectivity, the ECL response analysis of different miRNAs, one base and two bases mismatched miRNA-21 (M-1 and M-2), and their mixture was carried out under the same conditions. It can be seen from Figure 6C that the interfacial ECL responses are significantly lower than that of the specific response to the target miRNA, indicating excellent specificity of miRNA 21.

Detection of miRNA 21 in Different Cell Lysates. Due to the resistance to nonspecific adsorption of biomolecules in complex biological samples of the anti-fouling MBs, the designed analysis strategy can be used for detection of miRNA 21 in MCF-7 and HeLa cell lysate with different cell numbers. As shown in Figure 6D, the intensity of the ECL response increases with the increase of the amount of cells (10, 10^2, 10^3, 10^4, and 10^5 cells) and a good correlation is obtained, indicating the acceptable accuracy for miRNA detection in real complex samples. In addition, from the results, we can see that MCF-7 cells show higher expression than HeLa cells, which is consistent with previous research conclusions. The concentrations of the target substance in 10 MCF-7 cells and 10 HeLa cell lysates obtained with a Trizol reagent are about 1.52 ×

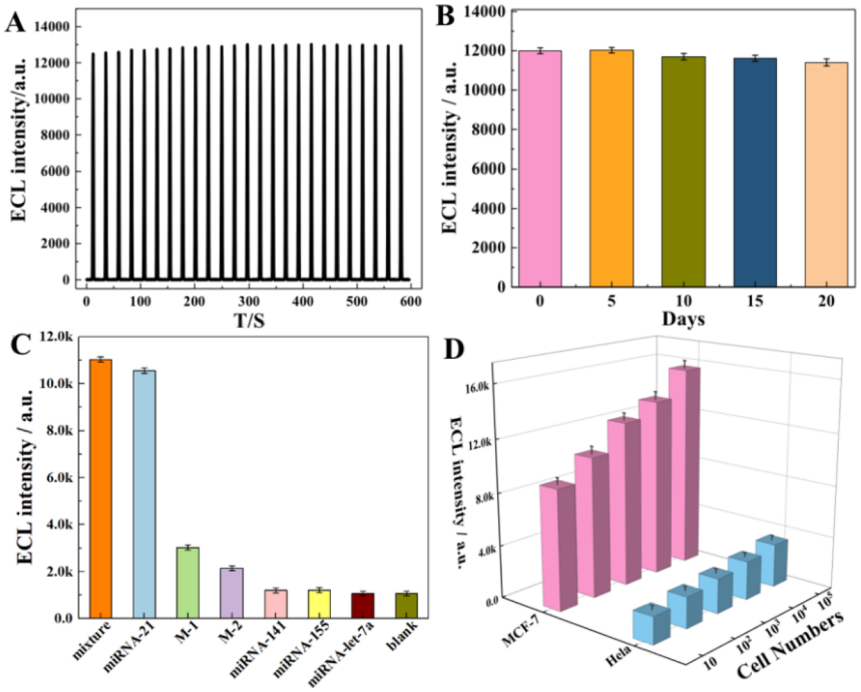

Figure 6. (A) ECL response after 25 consecutive scans. (B) ECL signal changes of the constructed sensor after storage for different days: 0, 5, 10, 15, and 20 days. (C) Selectivity of the constructed sensor to different interfering substances: M-1, M-2, miRNA 141, miRNA 155, and miRNA let-7a. (D) ECL response of this constructed biosensor to the cell lysate of different numbers: 10, 10^2, 10^3, 10^4, and 10^5 of HeLa and MCF-7.

https://doi.org/10.1021/acs.analchem.1c02186
Anal. Chem. 2021, 93, 10679−10687

10^{-13} and 1.40×10^{-17} M, respectively. Thus, the double signal amplification ECL analysis strategy based on anti-fouling MBs has potential application for analysis of miRNA 21 in other biological samples.

CONCLUSIONS

In conclusion, we proposed a signal amplification ECL biosensor based on anti-fouling MBs and TiO_2 NNs/PANI composite nanomaterials for the detection of miRNA in complex biological samples. The double signal amplification broadens the detection range and improves the sensitivity. The introduction of PANI with excellent conductivity makes up for the poorly conductive TiO_2 NNs, which can greatly enhance the ECL signal of $Ru(bpy)_2(cpaphen)^{2+}$. The newly designed dendrimer peptide exhibits pretty good resistance to nonspecific adsorption of biomolecules in complex biological samples' performance, so the modified MBs could realize anti-fouling magnetic separation and the subsequent ECL analysis shows high sensitivity and accuracy even in different cell lysates. We believe that the design principle presented herein represents a very promising advancement to construct anti-fouling biosensors and may be readily extended to a broad range of sensing devices for determination of targets in complex media.

ASSOCIATED CONTENT

Supporting Information

The Supporting Information is available free of charge at https://pubs.acs.org/doi/10.1021/acs.analchem.1c02186.

Reagents and materials; apparatus, preparation of TiO_2 NNs; fluorescence response; cell culture; characterization of TiO_2 NNs, MBs, MBs/dendritic peptide, and MBs/dendritic peptide/DNA; ECL mechanism of $Ru(bpy)_2(cpaphen)^{2+}$, TPrA, and TiO_2 NN ternary system; optimization of experimental conditions; calculation of the DNA connection density on the electrode surface; schematic diagram of the single signal amplification strategy with TiO_2 NNs; gel electrophoresis image of the single signal amplification system with TiO_2 NNs; ECL response of the single signal amplification system with the DNAzyme cycle or TiO_2 NNs (PDF)

AUTHOR INFORMATION

Corresponding Authors

Caifeng Ding − *Key Laboratory of Optic-electric Sensing and Analytical Chemistry for Life Science, Ministry of Education; Shandong Key Laboratory of Biochemical Analysis; Key Laboratory of Analytical Chemistry for Life Science in Universities of Shandong; College of Chemistry and Molecular Engineering, Qingdao University of Science and Technology, Qingdao 266042, PR China;* orcid.org/0000-0002-5281-0158; Email: dingcaifeng@qust.edu.cn

Xiliang Luo − *Key Laboratory of Optic-electric Sensing and Analytical Chemistry for Life Science, Ministry of Education; Shandong Key Laboratory of Biochemical Analysis; Key Laboratory of Analytical Chemistry for Life Science in Universities of Shandong; College of Chemistry and Molecular Engineering, Qingdao University of Science and Technology, Qingdao 266042, PR China;* orcid.org/0000-0001-6075-7089; Email: xiliangluo@qust.edu.cn

Authors

Qiuxia Hao − *Key Laboratory of Optic-electric Sensing and Analytical Chemistry for Life Science, Ministry of Education; Shandong Key Laboratory of Biochemical Analysis; Key Laboratory of Analytical Chemistry for Life Science in Universities of Shandong; College of Chemistry and Molecular Engineering, Qingdao University of Science and Technology, Qingdao 266042, PR China*

Qingzhang Xu − *Key Laboratory of Optic-electric Sensing and Analytical Chemistry for Life Science, Ministry of Education; Shandong Key Laboratory of Biochemical Analysis; Key Laboratory of Analytical Chemistry for Life Science in Universities of Shandong; College of Chemistry and Molecular Engineering, Qingdao University of Science and Technology, Qingdao 266042, PR China*

Shuyan Niu − *Key Laboratory of Optic-electric Sensing and Analytical Chemistry for Life Science, Ministry of Education; Shandong Key Laboratory of Biochemical Analysis; Key Laboratory of Analytical Chemistry for Life Science in Universities of Shandong; College of Chemistry and Molecular Engineering, Qingdao University of Science and Technology, Qingdao 266042, PR China*

Complete contact information is available at: https://pubs.acs.org/10.1021/acs.analchem.1c02186

Notes

The authors declare no competing financial interest.

ACKNOWLEDGMENTS

The authors greatly acknowledge support of the National Natural Science Foundation of China (22074074, 21974075), the Natural Science Foundation of Shandong Province (ZR2019BB055), the Taishan Scholar Program of Shandong Province of China (Grant ts20110829), and the Qingdao Science and Technology Demonstration Guidance Project (20-3-4-53-nsh).

REFERENCES

(1) Meng, L. Y.; Liu, C. C.; Lv, J. H.; Zhao, Q.; Deng, S. Q.; Wang, G. G.; Qiao, J.; Zhang, C. Y.; Zhen, L. X.; Lu, Y.; Li, W. S.; Zhang, Y. Z.; Pestell, R. G.; Fan, H. M.; Chen, Y. H.; Liu, Z. M.; Yu, Z. R. *Nat. Commun.* **2017**, *8*, 13964−13974.

(2) Ghini, F.; Rubolino, C.; Climent, M.; Simeone, I.; Marzi, M. J.; Nicassio, F. *Nat. Commun.* **2018**, *9*, 3119−3134.

(3) Yang, F. M.; Ning, Z. Q.; Ma, L.; Liu, W. T.; Shao, C. C.; Shu, Y. Q.; Shen, H. *Mol. Cancer* **2017**, *16*, 148−158.

(4) Saadatpour, L.; Fadaee, E.; Fadaei, S.; Mansour, R. N.; Mohammadi, M.; Mousavi, S.; Goodarzi, M.; Verdi, J.; Mizaei, H. *Cancer Gene Ther.* **2016**, *23*, 415−418.

(5) Martens-Uzunova, E. S.; Jalava, S. E.; Dits, N. F.; Leenders, G. V.; Moller, S.; Trapman, J.; Bangma, C. H.; Lieman, T.; Visakorpi, T.; Jenster, G. *Oncogene* **2012**, *31*, 978−991.

(6) Yu, C. Y.; Yin, B. C.; Wang, S. L.; Xu, Z. G.; Ye, B. C. *Anal. Chem.* **2014**, *86*, 7214−7218.

(7) Tian, H.; Sun, Y.; Liu, C.; Duan, X.; Tang, W.; Li, Z. *Anal. Chem.* **2016**, *88*, 11384−11389.

(8) Yin, J. Q.; Zhao, R. C.; Morris, K. V. *Trends Biotechnol.* **2008**, *26*, 70−76.

(9) Dong, J.; Chen, G. Y.; Wang, W.; Huang, X.; Peng, H. P.; Pu, Q. L.; Du, F.; Cui, X.; Deng, Y.; Tang, Z. *Anal. Chem.* **2018**, *90*, 7107−7111.

(10) Roy, S.; Soh, J. H.; Ying, J. Y. *Biosens. Bioelectron.* **2016**, *75*, 238−246.

(11) Li, D.; Xia, L.; Zhou, Q. J.; Wang, L.; Chen, D. M.; Gao, X.; Li, Y. *Anal. Chem.* **2020**, *92*, 12769−12773.

(12) Sun, Y. D.; Shi, L.; Wang, Q. W.; Mi, L.; Li, T. *Anal. Chem.* **2019**, *91*, 3652−3658.
(13) Zhang, Y.; Chai, Y. Q.; Wang, H. J.; Yuan, R. *Anal. Chem.* **2019**, *91*, 14368−14374.
(14) Chen, X.; Liu, Y. Z.; Xu, L. M.; Wang, Y.; Li, R.; Sun, P. M.; Lin, Z. Y.; Yang, H. H. *Anal. Chem.* **2019**, *91*, 13712−13719.
(15) Sun, Y. D.; Fang, L.; Zhang, Z.; Yi, Y.; Liu, S. J.; Chen, Q.; Zhang, J.; Zhang, C.; He, L. F.; Zhang, K. *Anal. Chem.* **2021**, *91*, 7516−7523.
(16) Zhang, X.; Nie, Y. X.; Zhang, Q.; Liang, Z. H.; Wang, P. L.; Ma, Q. *Chem. Eng. J.* **2021**, *411*, 128428.
(17) Sun, Y. D.; Fang, L.; Zhang, Z.; Yi, Y.; Liu, S. J.; Chen, Q.; Zhang, J.; Zhang, C.; He, L. F.; Zhang, K. *Anal. Chem.* **2021**, *93*, 7516−7522.
(18) Zhao, J. W.; Luo, J. H.; Liu, D.; He, Y.; Li, Q.; Chen, S. H.; Yuan, R. *Sens. Actuators, B* **2020**, *316*, 128139−128146.
(19) Cheng, H.; Liu, J. Q.; Ma, W. J.; Duan, S. D.; Huang, J.; He, X. X.; Wang, K. M. *Anal. Chem.* **2018**, *90*, 12544−12552.
(20) Shang, J. H.; Li, C. X.; Li, F. Z.; Wang, Q.; Yuan, B. F.; Wang, F. A. *Anal. Chem.* **2021**, *93*, 2403−2410.
(21) Liu, L.; Liu, J. W.; Wu, H.; Wang, X. N.; Yu, R. Q.; Jiang, J. H. *Anal. Chem.* **2018**, *90*, 1502−1505.
(22) Zhou, W. H.; Saran, R.; Liu, J. W. *Chem. Rev.* **2017**, *117*, 8272−8325.
(23) Chen, F.; Bai, M.; Cao, K.; Zhao, Y.; Cao, X. W.; Wei, J.; Wu, N.; Li, J.; Wang, L. H.; Fan, C. H.; Zhao, Y. Z. *ACS Nano* **2017**, *11*, 11908−11914.
(24) Wang, W. J.; Satyavolu, N. S. R.; Wu, Z. K.; Zhang, J. R.; Zhu, J. J.; Lu, Y. *Angew. Chem., Int. Ed.* **2017**, *56*, 6798−6802.
(25) Yang, Y. J.; Huang, J.; Yang, X. H.; He, X. X.; Quan, K.; Xie, N. L.; Ou, M.; Wang, K. M. *Anal. Chem.* **2017**, *89*, 5850−5856.
(26) Cao, W. D.; Ferrance, J. P.; Demas, J.; Landers, J. P. *J. Am. Chem. Soc.* **2006**, *128*, 7572−7578.
(27) Cui, C.; Chen, Y.; Jiang, D. C.; Chen, H. Y.; Zhang, J. R.; Zhu, J. J. *Anal. Chem.* **2019**, *91*, 1121−1125.
(28) Wang, C.; Zhang, N.; Li, Y. Y.; Yang, L.; Wei, D.; Yan, T.; Ju, H. X.; Du, B.; Wei, Q. *Sens. Actuators, B* **2019**, *291*, 319−328.
(29) Jiang, X. Y.; Wang, H. J.; Chai, Y. Q.; Shi, W. B.; Yuan, R. *Anal. Chem.* **2020**, *92*, 8992−9000.
(30) Lei, Y. M.; Zhou, J.; Chai, Y. Q.; Zhou, Y.; Yuan, R. *Anal. Chem.* **2018**, *90*, 12270−12277.
(31) Liao, H. X.; Zhou, Y.; Chai, Y. Q.; Yuan, R. *Biosens. Bioelectron.* **2018**, *114*, 10−14.
(32) Zhang, R.; Zhong, X.; Chen, A. Y.; Liu, J. L.; Li, S. K.; Chai, Y. Q.; Zhuo, Y.; Yuan, R. *Anal. Chem.* **2019**, *91*, 3681−3686.
(33) Hu, Y. C.; Liang, B.; Fang, L.; Ma, G. L.; Yang, G.; Zhu, Q.; Chen, S. F.; Ye, X. S. *Langmuir* **2016**, *32*, 11763−11770.
(34) Nowinski, A. K.; Sun, F.; White, A. D.; Keefe, A. J.; Jiang, S. Y. *J. Am. Chem. Soc.* **2012**, *134*, 6000−6005.
(35) Rio, J. S.; Henry, O. Y.; Jolly, P.; Ingber, D. E. *Nat. Nanotechnol.* **2019**, *14*, 1143−1149.
(36) Li, Y.; Han, R.; Chen, M.; Zhang, L. Y.; Wang, G. X.; Luo, X. L. *Anal. Chem.* **2021**, *93*, 4326−4333.
(37) Xu, Z. Y.; Han, R.; Liu, N. Z.; Gao, F. X.; Luo, X. L. *Sens. Actuators, B* **2020**, *319*, 128253−128259.
(38) Ma, L. Z.; Jayachandran, S.; Li, Z. M.; Song, Z.; Wang, W.; Luo, X. L. *J. Electroanal. Chem.* **2019**, *840*, 272−278.
(39) Li, C. X.; Liu, C. J.; Li, M. L.; Xu, X.; Li, S. Z.; Qi, W.; Su, R. X.; Yu, J. *Biomacromolecules* **2020**, *21*, 2087−2095.
(40) Chen, S. F.; Cao, Z. Q.; Jiang, S. Y. *Biomaterials* **2009**, *30*, 5892−5896.
(41) Liu, N. Z.; Song, J. Y.; Lu, Y. W.; Davis, J. J.; Gao, F. X.; Luo, X. L. *Anal. Chem.* **2019**, *91*, 8334−8340.
(42) Li, Y. X.; Wang, L.; Ding, C. F.; Luo, X. L. *Biosens. Bioelectron.* **2019**, *142*, 111553.
(43) Ding, C. F.; Li, Y. X.; Wang, L.; Luo, X. L. *Anal. Chem.* **2019**, *91*, 983−989.
(44) Ding, C. F.; Wang, X. Y.; Luo, X. L. *Anal. Chem.* **2019**, *91*, 15846−15852.
(45) Gu, S. T.; Shi, X. M.; Zhang, D.; Fan, G. C.; Luo, X. L. *Anal. Chem.* **2021**, *93*, 2706−2712.
(46) Song, Z.; Chen, M.; Ding, C. F.; Luo, X. L. *Anal. Chem.* **2020**, *92*, 5795−5802.
(47) Cui, M.; Ma, Y. H.; Wang, L.; Wang, Y.; Wang, S.; Luo, X. L. *TrAC, Trends Anal. Chem.* **2020**, *127*, 115903−115909.
(48) Castaneda, A. D.; Brenes, N. J.; Kondajji, A.; Crooks, R. M. *J. Am. Chem. Soc.* **2017**, *139*, 7657−7664.
(49) Liang, C. P.; Ma, P. Q.; Liu, H.; Guo, X. G.; Yin, B. C.; Ye, B. C. *Angew. Chem., Int. Ed.* **2017**, *56*, 9077−9081.
(50) Chen, J. X.; Zhuo, Y.; Peng, X.; Chai, Y. Q.; Yuan, R.; Liang, W. B. *Anal. Chem.* **2019**, *91*, 14125−14132.
(51) Xia, Y. K.; Wang, L. L.; Li, J.; Yan, A.; Lei, Y.; Yang, S.; Yang, H. H.; Chen, J. H. *Anal. Chem.* **2018**, *90*, 8969−8976.

https://doi.org/10.1021/acs.analchem.1c02186
Anal. Chem. 2021, 93, 10679−10687